RESEARCH REPORTS
Biological

E. Le Norcy[1,2], S.-Y. Kwak[1,2], F.B. Wiedemann-Bidlack[1,2], E. Beniash[3], Y. Yamakoshi[4], J.P. Simmer[4], and H.C. Margolis [1,2]*

[1]Department of Biomineralization, The Forsyth Institute, 245 First Street, Cambridge, MA 02142, USA; [2]Department of Developmental Biology, Harvard School of Dental Medicine, Boston, MA, USA; [3]Department of Oral Biology, University of Pittsburgh, PA, USA; and [4]Dental Research Laboratory, University of Michigan, Ann Arbor, MI, USA; *corresponding author, hmargolis@forsyth.org

J Dent Res 90(9):1091-1097, 2011

Leucine-rich Amelogenin Peptides Regulate Mineralization *in vitro*

ABSTRACT

Amelogenin's capacity to regulate enamel formation is related to its conserved N- and C-terminal domains, its ability to self-assemble, and its ability to stabilize amorphous calcium phosphate (ACP) – a capacity enhanced by amelogenin phosphorylation. This *in vitro* study provides further insight into amelogenin function, using variations of the Leucine-Rich Amelogenin Peptide (LRAP), an alternative splice product comprised solely of amelogenin's N- and C-terminal domains. Peptide self-assembly was studied by dynamic light-scattering and transmission electron microscopy (TEM). TEM, selected area electron diffraction, and Fourier transform-infrared spectroscopy were also used to determine the effect of phosphorylated and non-phosphorylated LRAP on calcium phosphate formation. Results show that phosphorylated and non-phosphorylated LRAP can self-assemble into chain-like structures in a fashion dependent on the C-terminal domain. Notably, this capacity was enhanced by added calcium and to a much greater degree for phosphorylated LRAP. Furthermore, phosphorylated LRAP was found to stabilize ACP and prevent its transformation to hydroxyapatite (HA), while aligned HA crystals formed in the presence of non-phosphorylated LRAP. The N- and C-terminal amelogenin domains in non-phosphorylated LRAP are, therefore, sufficient to guide ACP transformation into ordered bundles of apatite crystals, making LRAP an excellent candidate for biomimetic approaches for enamel regeneration.

KEY WORDS: amelogenin, calcium, enamel, LRAP, mineralization, self-assembly.

DOI: 10.1177/0022034511411301

Received January 31, 2011; Last revision March 26, 2011; Accepted April 27, 2011

A supplemental appendix to this article is published electronically only at http://jdr.sagepub.com/supplemental.

INTRODUCTION

Amelogenin, the predominant enamel matrix protein, is essential for proper enamel formation (Gibson *et al*., 2001) and is believed to play key roles in regulating nucleation, growth, morphology, and organization of developing enamel mineral phases (Moradian-Oldak *et al*., 1998; Beniash *et al*., 2005; Margolis *et al*., 2006; Tarasevich *et al*., 2007; Wang *et al*., 2007; Kwak *et al*., 2009). Amelogenin is composed of a tyrosine-rich N-terminal domain (called TRAP – tyrosine-rich amelogenin peptide), containing the protein's only phosphorylation site, a large central hydrophobic domain, and a highly conserved hydrophilic C-terminus. Amelogenin has been shown to assemble into nanoparticles, frequently called nanospheres, and higher-order chain-like structures under specific conditions (Fincham *et al*., 1995; Aichmayer *et al*., 2005, 2010; Beniash *et al*., 2005; Wiedemann-Bidlack *et al*., 2007, 2011).

The Leucine-Rich Amelogenin Peptide (LRAP) is an alternative splicing product of the amelogenin gene expressed throughout enamel development (Yuan *et al*., 1996). Porcine LRAP is comprised of 56 amino acids: the 33 N-terminal (including the phosphorylation site) and 23 C-terminal amino acids (including the hydrophilic domain) of full-length amelogenin (Fincham and Moradian-Oldak, 1993). The N-terminal and C-terminal domains of full-length amelogenin have been shown to play essential roles in proper enamel mineral formation (Paine *et al*., 2003a,b).

Although its role in amelogenesis is unclear, LRAP shares some properties with full-length amelogenin. LRAP, like amelogenin (*e.g*., rH175), forms nanospheres, as shown for fluoroapatite (Habelitz *et al*., 2006) or surfactant-coated gold surfaces (Tarasevich *et al*., 2010), and appears to interact with hydroxyapatite through its C-terminus (Shaw *et al*., 2004), although this domain is not solely responsible for mineral binding (Shaw *et al*., 2008). LRAP is also processed during secretory amelogenesis by enamelysin, resulting in the removal of 16 C-terminal amino acids, and by kallikrein-4 during the maturation stage (Nagano *et al*., 2009). The C-terminal domain of amelogenin has been shown to be essential for protein self-assembly in enamel (Paine *et al*., 2003b), the formation of chain-like structures (Wiedemann-Bidlack *et al*., 2007, 2011), and for guiding the generation of parallel arrays of apatitic crystals *in vitro* (Beniash *et al*., 2005; Kwak *et al*., 2009). Furthermore, LRAP has been shown to partially rescue the amelogenin knockout enamel phenotype (Gibson *et al*., 2009), as was also shown with the full-length molecule (Li *et al*., 2008). This was not the case, however, when amelogenin lacking the C-terminus was used, again indicating that the C-terminal domain is essential for normal enamel development (Pugach *et al*., 2010).

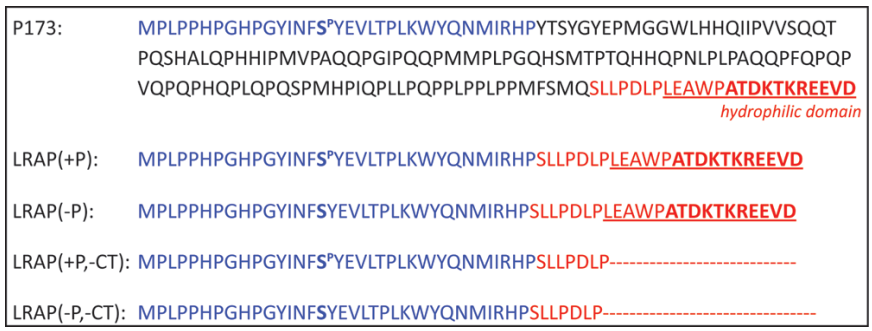

Figure 1. Amino acid sequence of the full-length native porcine amelogenin P173, and indicated relationship to the synthetic forms of LRAP used in the present study.

We carried out the present study to examine the self-assembly behavior of LRAP, as a function of pH and calcium addition, and to determine the effect of LRAP on spontaneous calcium phosphate formation *in vitro*. More specifically, we performed studies to assess the roles of the single phosphate group and the hydrophilic C-terminus found in LRAP on self-assembly, and the effect of LRAP phosphorylation on mineral formation. The phosphorylation of amelogenin has recently been shown to have a marked effect on mineralization *in vitro* (Kwak *et al*., 2009; Wiedemann-Bidlack *et al*., 2011). Studies were conducted with synthetic forms of LRAP with [LRAP(+P)] and without [LRAP(-P)] phosphorylation, and also without the 16-amino-acid C-terminus [*i.e.*. LRAP(+P,-CT) and LRAP(-P,-CT)] (Fig. 1).

MATERIALS & METHODS

Preparation of LRAP Peptides

Variations of the porcine LRAP peptide (Fig. 1) were synthesized commercially (NEO Peptide, Cambridge, MA, USA) and re-purified, as previously described (Nagano *et al*., 2009). Lyophilized peptides were weighed and dissolved in distilled de-ionized water at room temperature to yield stock solutions of 5 mg/mL (pH ~ 3). Stock solutions were centrifuged (10,900 x *g*, 4°C, 20 min) just prior to use. All other solutions were first filtered (0.22-μm filter).

Dynamic Light-scattering (DLS) Experiments

We used dynamic light-scattering (DLS) to obtain information on the aggregation of LRAP peptides as a function of solution pH and/or the addition of calcium (see Appendix for additional information). Aliquots of peptides were mixed with MES (pH 4 – 6.5) or MOPS (pH 6.5 – 10) buffers to obtain final concentrations of 2 mg/mL and 20 mM buffer. Final pH adjustments were made with KOH, at 25°C or 37ºC. In selected experiments, calcium chloride was also added to yield a final concentration of 2.5 mM calcium.

Each DLS experiment (DynaPro MSXTC/12) was comprised of 8 measurements of 20 acquisitions (5 sec each) at 5-minute intervals at either 25°C or 37°C. The size (hydrodynamic radius, R_H) of LRAP particles in buffers at selected pH values and fixed temperatures was determined. DLS data were analyzed, as previously described (Wiedemann-Bidlack *et al*., 2007). The formation of very large aggregates or a gel-like phase was indicated by a jump in scattering intensity to values above the detection limit of the instrument.

TEM Analyses

Five-μL aliquots were taken immediately after DLS self-assembly experiments or at specified times from mineralization solutions (see below) and placed on carbon-coated Cu grids (Electron Microscopy Sciences, Hatfield, PA, USA). Duplicate grids were prepared from a minimum of 3 different experiments, and selected samples were negatively stained (30 sec) with 1% filtered phospho-tungstic acid (PTA) adjusted to the pH of the sample being examined. Images were obtained in bright-field and/or Selected Area Electron Diffraction (SAED) modes with a JEOL 1200 TEM microscope at 100 kV and captured by an AMT CCD camera (AMT, Danvers, MA, USA). Images were analyzed with ImageJ 1.43u software (NIH, Bethesda, MD, USA). Statistical analyses were conducted with SigmaStat v3.11 software (Systat Software, Inc., Chicago, IL, USA). ANOVA and Holm-Sidak comparison tests were performed ($\alpha = 0.05$, $p < 0.001$).

Mineralization Studies

Aliquots of calcium and pH-adjusted phosphate solutions (pH 11.3 ± 0.1) were sequentially added to peptide solutions, as previously reported (Kwak *et al*., 2009). Solutions were quickly adjusted to a final value of pH 7.4 at 37°C with KOH to yield final concentrations of 2.5 mM Ca, 1.5 mM P, and 2 mg/mL peptide (volume, 0.06 mL). The pH of each experimental solution was monitored continuously by means of a micro-combination pH electrode (MI-410, Microelectrodes Inc., Bedford, NH, USA). Each experiment ($n \geq 3$) was conducted in duplicate, with the duplicate tube being used for TEM analyses, as described above. The final pH of the latter sample was checked to confirm that it was similar to that of the other sample.

Fourier Transform-Infrared (FT-IR) Spectroscopy Analyses

Twenty-four-hour samples from selected mineralization experiments were concentrated, placed on KBr IR Cards (International Crystal Labs, Garfield, NJ, USA), and air-dried. FT-IR spectra (4000 to 450 cm^{-1}) of samples were recorded by means of a Multiscope FT-IR microscope (Perkin-Elmer), as reported (Kwak *et al*., 2009).

RESULTS

Effects of pH and Calcium on the Assembly of LRAP Peptides

At pH < 4 at 25°C, DLS analyses indicated that all LRAP forms appeared as small nanoparticles with R_H values ~1 nm (Fig. 2A). Under less acidic conditions of 4.5 < pH < 6, however, all LRAP

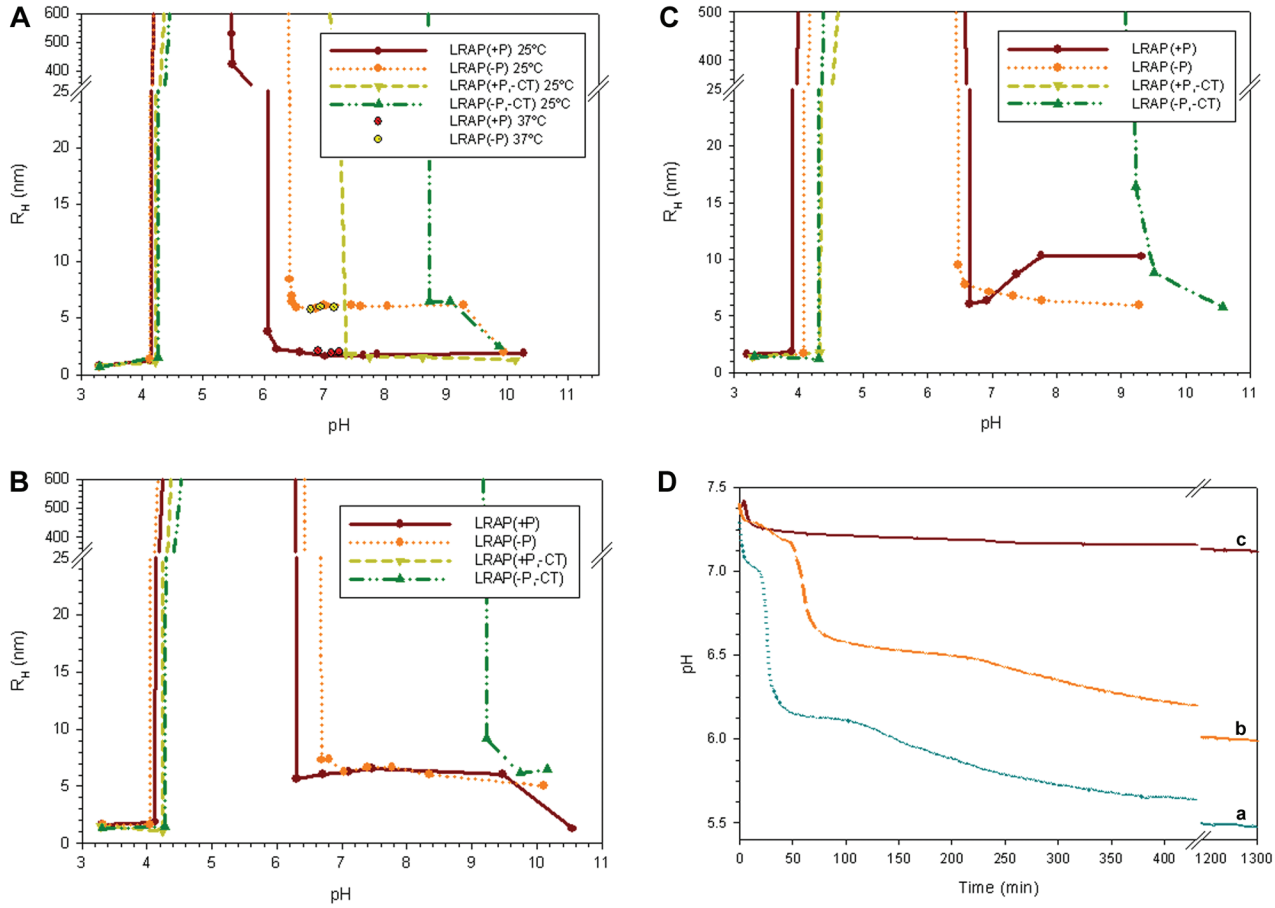

Figure 2. DLS analyses of pH-triggered self-assembly of LRAP(+P), LRAP(-P), LRAP(+P,-CT), and LRAP(-P,-CT) in 20 mM MES/MOPS buffer at 25°C (**A**), and with added 2.5 mM $CaCl_2$ at 25°C (**B**) and 37°C (**C**). Results obtained for LRAP(+P) and LRAP(-P) at selected pH values near neutrality at 37°C are also shown (A). In (A), (B) and (C), observed particle sizes (R_H) and off-scale scattering are indicated as a function of pH. Samples examined at pH ~3 (A, B, C) were prepared in DDW. In (**D**), changes in pH as a function of time were observed during mineralization experiments under conditions of spontaneous calcium phosphate precipitation (37°C, initial pH 7.4, vol 0.06 mL) over 24 hrs in the absence (**a**) and presence of LRAP(-P) (**b**) and LRAP(+P) (**c**).

peptides exhibited off-scale DLS scattering (Fig. 2A), corresponding to the formation of large particles or gel-like phases. Consistent with DLS findings, TEM analyses of LRAP(+P) and LRAP(+P, -CT) exhibited large spherical structures (~ 500 nm in diameter) at pH 5 (Figs. 3B, 3D), whereas LRAP(-P) and LRAP(-P,-CT) exhibited random extended gel-like phases (Figs. 3A, 3C). LRAP(+P) and LRAP(-P) were similarly found to have a tendency to form large aggregates over a wide range of concentrations (down to 0.125 mg/mL) at pH 5 (data not shown).

At pH 7.0 and 25°C, DLS showed that LRAP(+P) and LRAP(-P) formed small structures (R_H = 2-6 nm), whereas LRAP(+P,-CT) and LRAP(-P,-CT) still exhibited off-scale behavior (Fig. 2A). DLS findings similar to those found at 25°C were obtained for LRAP(+P) and LRAP(-P) at pH 7.0 at 37°C (Fig. 2A). TEM analyses of LRAP(-P) and LRAP(+P) at pH 7.0 at 25°C (Figs. 3E, 3F) and 37°C (Figs. 3M, 3N) revealed a mixture of isolated spherical nanoparticles (from 10 to 12 nm in diameter) and their assembly into chain-like structures (defined here as the linear association of 3 or more spheres with a discrete beginning and end). In contrast, TEM analyses of LRAP(-P,-CT) showed large isolated spheres and aggregates (Fig. 3G), while LRAP(+P,-CT) revealed similar large spheres interconnected in a web-like fashion through multiple connection points by thin threads that link one sphere to another (Fig. 3H). When LRAP(-P) was examined at pH 6.0 (Fig. 3P), chain-like structures and aggregates of chain-like structures predominated, with few isolated particles seen.

Relative to DLS findings in the absence of calcium (Fig. 2A), the addition of 2.5 mM Ca resulted in a notable change in particle sizes (R_H) for both LRAP(+P) and LRAP(+P,-CT) at 25ºC (Fig. 2B) and 37ºC (Fig. 2C). For LRAP(+P), R_H values increased from ~ 2 nm to 6-10 nm at pH > 6. A more dramatic effect was observed with LRAP(+P, -CT), where R_H values of ~2 nm, seen at pH > 7.4, increased to off-scale values upon the addition of calcium. In sharp contrast, calcium had relatively little effect on LRAP(-P) and LRAP(-P,-CT) assembly at either temperature (Figs. 2B, 2C). However, TEM analyses of both LRAP(-P) and LRAP(+P) at 37ºC revealed statistically significant ($p < 0.02$)

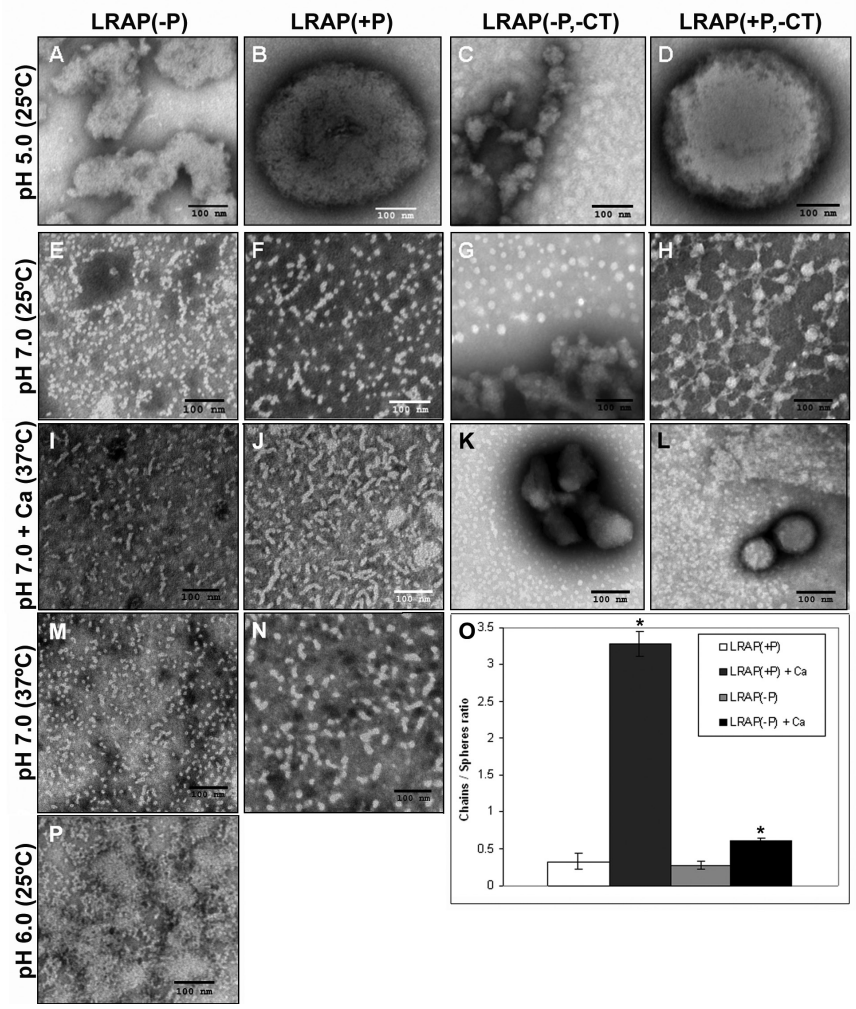

Figure 3. TEM images with PTA staining of LRAP(-P) (**A, E, I, M, P**), LRAP(+P) (**B, F, J, N**), LRAP(-P,-CT) (**C, G, K**), and LRAP(+P,-CT) (**D, H, L**) in 20 mM MES buffer at pH 5.0 (A-D), 20 mM MOPS buffer at pH 7.0 (E-H), and 20 mM MES buffer at pH 6.0 (P) at 25°C, and at pH 7.0 at 37°C without (M, N) and with (I-L) 2.5 mM $CaCl_2$. All protein concentrations were 2 mg/mL. Note that nanospheres and chain-like particles were observed at neutral pH with LRAP(-P) (E, M) and LRAP(+P) (F, N), but not with LRAP(-P,-CT) and LRAP(+P,-CT) (G, H). Chain-like particles were predominant with LRAP(+P) in the presence of calcium (J), indicating an assembly of the nanospheres into chains. **(O)** Comparison of the effect of added calcium on the ratio of chain-like structures to spheres of LRAP(+P) and LRAP(-P) at pH 7.0 and 37°C, under the same conditions used for I, J, M, and N. As shown and discussed in the text, the ratio of chain-like structures to spheres increased significantly ($p < 0.02$) for both LRAP(+P) and LRAP(-P) in the presence of calcium, and, to a greater extent, for LRAP(+P). We obtained results by counting [using cell count (Image J)] the numbers of isolated spheres and chains (n= 200 to 1200) on 5 representative TEM images from a minimum of 3 experiments. Scale bar in all images is 100 nm.

increases in the relative numbers of chain-like structures in the presence of calcium (Figs. 3I, 3J), in comparison with that seen in its absence (Figs. 3M, 3N). It was found (Fig. 3O) that, with added calcium, the ratio of the number of chain-like structures to isolated spheres at pH 7.0 increased by 10-fold for LRAP(+P) (from 0.32 ± 0.11 to 3.27 ± 0.16) and by 2.3-fold for LRAP(-P) (from 0.27 ± 0.06 to 0.62 ± 0.02). TEM analysis of LRAP(-P, -CT) (Fig. 3K) and LRAP(+P, -CT) (Fig. 3L), in the presence of calcium at pH 7.0 and 37ºC, revealed a mixture of smaller spheres and large aggregates.

Effects of LRAP(+P) and LRAP(-P) on Spontaneous Mineralization *in vitro*

Building on our self-assembly findings, which show that both LRAP(+P) and LRAP(-P) form chain-like structures, we investigated their effects on *in vitro* mineralization. In the control, a marked decrease in pH was observed over time (Fig. 2D). An initial plateau, seen until 30 min, corresponded to the presence of spherical particles of amorphous calcium phosphate (ACP), as observed with TEM. Mineral phase identification was based on SAED analyses (Fig. 4A, 30 min, inset) and known ACP morphology (Eanes, 2001; Mahamid *et al*., 2008), which were consistent with those of amorphous material. A marked decrease in pH was then observed that corresponded to the formation and growth of plate-like particles at 2 hrs (Fig. 4A, 2 hrs), followed by a slow decrease in pH up to 24 hrs that resulted in the formation of randomly arranged plate-like crystals (Fig. 4A, 24 hrs). SAED analyses (Fig. 4A, 24 hrs, inset) were consistent with the formation of hydroxyapatite (HA), as confirmed by FT-IR (Appendix Fig. 1). In the presence of LRAP(+P), after a small decrease in pH, only a slight pH change was observed for up to 24 hrs (Fig. 2D). TEM and SAED analyses showed that, in the presence of LRAP(+P) (Fig. 4C), spherical nanoparticles of ACP were present at 30 min and remained up to 24 hrs, as confirmed by FT-IR (Appendix Fig. 1). Although not characterized, smaller mineral particles were seen at 5 to 10 min that appeared to grow over time without transforming to HA. ACP particles observed in the presence of LRAP(+P) at 24 hrs were significantly smaller in diameter (26.2 ± 4.0 nm) than ACP particles observed in the control at 5-10 min (84 ± 5.2 nm). Similarly, LRAP(+P) was found to stabilize ACP particles for up to 24 hrs at lower concentrations down to 0.175 mg/mL (data not shown).

In the presence of LRAP(-P), a marked decrease in pH over time was also observed (Fig. 2D), similar to that seen in the control. However, a longer initial plateau of 1 hr was seen that again corresponded to the presence of spherical ACP particles (Fig. 4B). In the presence of LRAP(-P), however, bundles of ordered needle-

like mineral particles were seen at 2 hrs (Fig. 4B). Similar results were obtained with lower concentrations (down to 0.7 mg/mL) of LRAP(-P) (data not shown). These bundles of well-aligned crystals appeared to aggregate as the pH of the solution continued to decrease (Fig. 4B, 24 hrs). This phenomenon may be a result of peptide aggregation at lower pH values observed at 24 hrs (Fig. 2D), in comparison with the pH at 2 hrs, based on DLS (Fig. 2) and TEM (Fig. 3) findings. SAED analyses of isolated bundles of crystals collected at 2 hrs and 24 hrs (Fig. 4B, Appendix Fig. 2) were consistent with the formation of thin HA crystals aligned along their c-axes. TEM images of negatively stained samples at 24 hrs suggested an alignment of LRAP(-P) nanospheres along the edges of what are assumed to be crystals (Appendix Fig. 3). Between crystals, LRAP(-P) nanospheres appeared to aggregate over time, consistent with DLS results and pH values observed at these time-points.

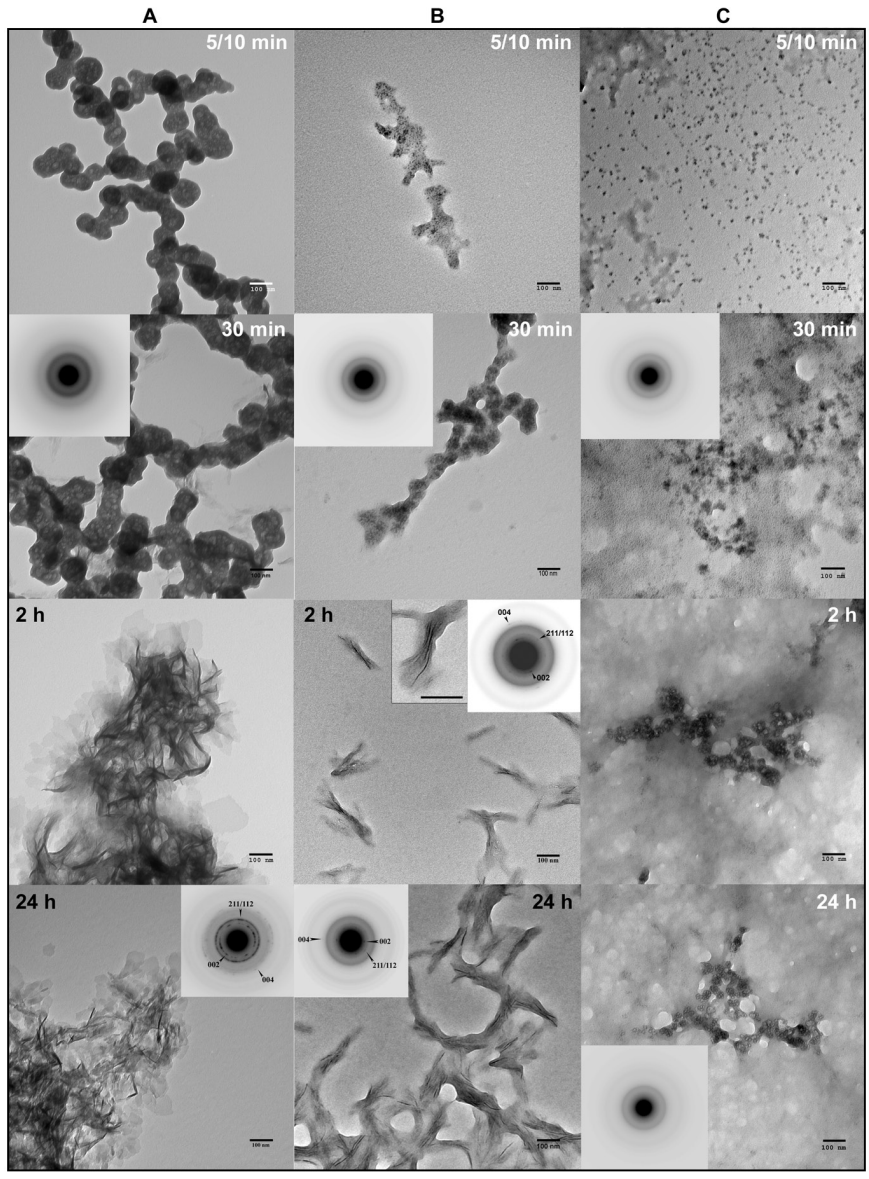

Figure 4. TEM and SAED analyses of mineral phases formed during mineralization experiments in the absence and presence of added peptides (2 mg/mL): **(A)** control (no added peptide), **(B)** LRAP(-P), and **(C)** LRAP(+P) at different time-points. As shown, amorphous calcium phosphate (ACP) was initially formed in the control and in the presence of LRAP(+P) and LRAP(-P), based on the observed (insets) selected area diffraction (SAED) patterns at 30 min and characteristic spherical morphology. At 2 hrs, randomly arranged plate-like crystals were found in the control (A), whereas ordered bundles of needle-like crystals were formed in the presence of LRAP(-P) (B). Similar structures were also seen at 24 hrs. SAED analyses of control samples at 24 hrs (A) were consistent with randomly oriented hydroxyapatite crystals, while SAED analyses of isolated bundles of crystals obtained in the presence of LRAP(-P) showed narrow arcs corresponding to 002 and 004 reflections, indicating that the crystals of hydroxyapatite were aligned parallel in the c-axis direction. In contrast to these findings, in the presence of LRAP(+P) (C), ACP remained for up to 24 hrs. Mineral phase identification by SAED was confirmed by FT-IR (Appendix Fig. 1). Scale bar in all images is 100 nm.

DISCUSSION

Results obtained indicate that porcine LRAP shares striking similarities with amelogenin with respect to its assembly behavior and effect on calcium phosphate formation *in vitro*. At neutral pH, LRAP(+P) and LRAP(-P) assemble to form chain-like structures composed of nanospheres, in a fashion similar to that seen for full-length amelogenins (Wiedemann-Bidlack *et al*., 2007, 2011). Although previously shown to form nanospheres (Habelitz *et al*., 2006; Tarasevich *et al*., 2010), the capacity of LRAP nanospheres to assemble into chain-like structures has not been previously shown. Notably, we have found that the addition of calcium has a major effect on the higher-order assembly of LRAP(+P) by enhancing the assembly of LRAP(+P) nanospheres into chain-like structures at pH 7.0, whereas calcium had a much smaller effect on LRAP(-P) assembly. Again, similar to that seen for full-length amelogenin (Paine *et al*., 2003b; Wiedemann-Bidlack *et al*., 2007), LRAP loses its ability to assemble into chain-like structures at neutral pH when the C-terminal amino-acids are absent, even in the presence of calcium, confirming the importance of the C-terminus in higher-order amelogenin assembly (Paine *et al*., 2003b).

We have also found that the phosphorylated form of LRAP, LRAP(+P), can stabilize ACP particles *in vitro* and prevent their transformation into hydroxyapatite. These findings are similar to those obtained with native phosphorylated full-length (P173)

(Wiedemann-Bidlack *et al*., 2011) and cleaved (P148) (Kwak *et al*., 2009) porcine amelogenins, as well as LRAP(+P,-CT) (Le Norcy *et al*., 2011). These collective results suggest an important role of the sole phosphate group found in native amelogenins in the regulation of crystal formation *in vivo*. Although direct evidence is lacking, the transformation of ACP into hydroxyapatite crystals *in vivo* might be regulated by the dephosphorylation (Brookes *et al*., 1998) or degradation (Robinson *et al*., 2003) of amelogenin to less mineral-interactive forms. The ability of native amelogenins to stabilize ACP formation, nevertheless, is consistent with recent findings showing that ACP forms initially in developing enamel as linear arrays, which subsequently transform into apatitic crystals (Beniash *et al*., 2009).

The non-phosphorylated peptide LRAP(-P), however, was shown to guide the formation of bundles of well-aligned needle-like apatitic crystals, as was previously found for recombinant full-length amelogenins (Beniash *et al*., 2005; Kwak *et al*., 2009). Our earlier findings demonstrated that full-length recombinant porcine amelogenin rP172 has the ability to transiently stabilize ACP nanoparticles and guide their alignment into linear arrays during the formation of ordered bundles of needle-like crystals *in vitro* (Kwak *et al*., 2009). Notably, our TEM results suggest that nanospheres of LRAP(-P) are aligned along the edges of what appear to be nascent crystals (Appendix Fig. 3). Although further studies are needed, this observation may be related to the ability of LRAP(-P) to assemble into elongated chain-like structures comprised of nanospheres, particularly in the presence of calcium at pH < 7.4. Thus, these peptide chains may serve to align the growth of apatitic crystals along their c-axis.

In conclusion, we have shown that LRAP and analogous structural variants have striking similarities with full-length and cleaved forms of amelogenin. LRAP can assemble into chains of nanospheres and regulate *in vitro* mineralization. We have shown that the N-terminal and C-terminal amelogenin domains in non-phosphorylated LRAP(-P) are sufficient to guide ACP transformation into ordered bundles of apatite crystals. Although its role in enamel formation is unclear, LRAP appears to be an ideal candidate for use in biomimetic approaches for enamel regeneration.

ACKNOWLEDGMENTS

This work was supported by NIDCR grant R01-DE016376 (HCM). The authors declare no potential conflicts of interest with respect to the authorship and/or publication of this article.

REFERENCES

Aichmayer B, Margolis HC, Sigel R, Yamakoshi Y, Simmer JP, Fratzl P (2005). The onset of amelogenin nanosphere aggregation studied by small-angle x-ray scattering and dynamic light scattering. *J Struct Biol* 151:239-249.

Aichmayer B, Wiedemann-Bidlack FB, Gilow C, Simmer J, Yamakoshi Y, Emmerling F, *et al*. (2010). Amelogenin nanoparticles in suspension: deviations from spherical shape and pH-dependent aggregation. *Biomacromolecules* 11:369-376.

Beniash E, Simmer JP, Margolis HC (2005). The effect of recombinant mouse amelogenins on the formation and organization of hydroxyapatite crystals *in vitro*. *J Struct Biol* 149:182-190.

Beniash E, Metzler RA, Lam RS, Gilbert PU (2009). Transient amorphous calcium phosphate in forming enamel. *J Struct Biol* 166:133-143.

Brookes SJ, Kirkham J, Shore RC, Bonass WA, Robinson C (1998). Enzyme compartmentalization during biphasic enamel matrix processing. *Connect Tissue Res* 39:89-99.

Eanes ED (2001). Amorphous calcium phosphate. In: *Octacalcium phosphate*. Chow LC, Eanes ED, editors. Basel: S. Karger AG, p. 167.

Fincham AG, Moradian-Oldak J (1993). Amelogenin post-translational modifications: carboxy-terminal processing and the phosphorylation of bovine and porcine "TRAP" and "LRAP" amelogenins. *Biochem Biophys Res Commun* 197:248-255.

Fincham AG, Moradian-Oldak J, Diekwisch TG, Lyaruu DM, Wright JT, Bringas P Jr, *et al*. (1995). Evidence for amelogenin "nanospheres" as functional components of secretory-stage enamel matrix. *J Struct Biol* 115:50-59.

Gibson CW, Yuan ZA, Hall B, Longenecker G, Chen E, Thyagarajan T, *et al*. (2001). Amelogenin-deficient mice display an amelogenesis imperfecta phenotype. *J Biol Chem* 276:31871-31875.

Gibson CW, Li Y, Daly B, Suggs C, Yuan ZA, Fong H, *et al*. (2009). The leucine-rich amelogenin peptide alters the amelogenin null enamel phenotype. *Cells Tissues Organs* 189:169-174.

Habelitz S, DenBesten PK, Marshall SJ, Marshall GW, Li W (2006). Self-assembly and effect on crystal growth of the leucine-rich amelogenin peptide. *Eur J Oral Sci* 114(Suppl 1):315-319.

Kwak SY, Wiedemann-Bidlack FB, Beniash E, Yamakoshi Y, Simmer JP, Litman A, *et al*. (2009). Role of 20-kDa amelogenin (P148) phosphorylation in calcium phosphate formation *in vitro*. *J Biol Chem* 284:18972-18979.

Le Norcy E, Kwak SY, Wiedemann-Bidlack FB, Beniash E, Yamakoshi Y, Simmer JP, *et al*. (2011). Potential role of the amelogenin N-terminus in the regulation of calcium phosphate formation *in vitro*. *Cells Tissues Organs* [Epub ahead of print May 13, 2011]. In Press.

Li Y, Suggs C, Wright JT, Yuan ZA, Aragon M, Fong H, *et al*. (2008). Partial rescue of the amelogenin null dental enamel phenotype. *J Biol Chem* 283:15056-15062.

Mahamid J, Sharir A, Addadi L, Weiner S (2008). Amorphous calcium phosphate is a major component of the forming fin bones of zebrafish: indications for an amorphous precursor phase. *Proc Natl Acad Sci USA* 105:12748-12753.

Margolis HC, Beniash E, Fowler CE (2006). Role of macromolecular assembly of enamel matrix proteins in enamel formation. *J Dent Res* 85:775-793.

Moradian-Oldak J, Tan J, Fincham AG (1998). Interaction of amelogenin with hydroxyapatite crystals: an adherence effect through amelogenin molecular self-association. *Biopolymers* 46:225-238.

Nagano T, Kakegawa A, Yamakoshi Y, Tsuchiya S, Hu JC, Gomi K, *et al*. (2009). Mmp-20 and Klk4 cleavage site preferences for amelogenin sequences. *J Dent Res* 88:823-828.

Paine ML, Luo W, Zhu DH, Bringas P Jr, Snead ML (2003a). Functional domains for amelogenin revealed by compound genetic defects. *J Bone Miner Res* 18:466-472.

Paine ML, Wang HJ, Snead ML (2003b). Amelogenin self-assembly and the role of the proline located within the carboxyl-teleopeptide. *Connect Tissue Res* 44(Suppl 1):52-57.

Pugach MK, Li Y, Suggs C, Wright JT, Aragon MA, Yuan ZA, *et al*. (2010). The amelogenin C-terminus is required for enamel development. *J Dent Res* 89:165-169.

Robinson C, Shore RC, Wood SR, Brookes SJ, Smith DA, Wright JT, *et al*. (2003). Subunit structures in hydroxyapatite crystal development in enamel: implications for amelogenesis imperfecta. *Connect Tissue Res* 44(Suppl 1):65-71.

Shaw WJ, Campbell AA, Paine ML, Snead ML (2004). The COOH terminus of the amelogenin, LRAP, is oriented next to the hydroxyapatite surface. *J Biol Chem* 279:40263-40266.

Shaw WJ, Ferris K, Tarasevich B, Larson JL (2008). The structure and orientation of the C-terminus of LRAP. *Biophys J* 94:3247-3257.

Tarasevich BJ, Howard CJ, Larson JL, Snead ML, Simmer JP, Paine M, *et al*. (2007). The nucleation and growth of calcium phosphate by amelogenin. *J Cryst Growth* 304:407-415.

Tarasevich BJ, Lea S, Shaw WJ (2010). The leucine rich amelogenin protein (LRAP) adsorbs as monomers or dimers onto surfaces. *J Struct Biol* 169:266-276.

Wang L, Guan X, Du C, Moradian-Oldak J, Nancollas GH (2007). Amelogenin promotes the formation of elongated apatite microstructures in a controlled crystallization system. *J Phys Chem C Nanomater Interfaces* 111:6398-6404.

Wiedemann-Bidlack FB, Beniash E, Yamakoshi Y, Simmer JP, Margolis HC (2007). pH triggered self-assembly of native and recombinant amelogenins under physiological pH and temperature *in vitro*. *J Struct Biol* 160:57-69.

Wiedemann-Bidlack FB, Kwak SY, Beniash E, Yamakoshi Y, Simmer JP, Margolis HC (2011). Effects of phosphorylation on the self-assembly of native full-length porcine amelogenin and its regulation of calcium phosphate formation *in vitro*. *J Struct Biol* 173:250-260.

Yuan ZA, Collier PM, Rosenbloom J, Gibson CW (1996). Analysis of amelogenin mRNA during bovine tooth development. *Arch Oral Biol* 41:205-213.